3 Biotech (2017) 7:89
DOI 10.1007/s13205-017-0731-8

ORIGINAL ARTICLE

Enhanced antimicrobial and anticancer properties of ZnO and TiO_2 nanocomposites

CH. Shilpa Chakra[1] · V. Rajendar[2] · K. Venkateswara Rao[3] · Mirgender Kumar[2]

Received: 2 December 2016 / Accepted: 30 January 2017 / Published online: 26 May 2017

Abstract The study describes the antibacterial and anticancer activities of a nanocomposite prepared by mixing zinc oxide and titanium dioxide nanoparticles. The particle mixtures were analyzed by X-ray diffraction, Field emission scanning electron microscopy, transmission electron microscopy, Fourier transform infrared spectroscopy, and dynamic light scattering techniques. Thus, analyzed samples were subject to disc diffusion method at various concentrations to analyze their antibacterial activities against two Gram-positive and two Gram-negative bacteria. The same samples were then analyzed for their anticancer activities on four different cell lines. The results indicate a synergistic effect of the nanocomposite on both antibacterial and anticancer properties when compared to their individual counterparts.

Keywords Nanocomposite · Zinc oxide · Titanium dioxide · Nanoparticles · Anticancer · Antibacterial

✉ V. Rajendar
rajendar.nano@gmail.com

[1] Center for Nanoscience and Technology, Institute of Science and Technology, Jawaharlal Nehru Technological University Hyderabad, Hyderabad, Telangana 500085, India

[2] Department of Electronic Engineering, Yeungnam University, Gyeongsan-si, Gyeongsangbuk-do 38541, Republic of Korea

[3] Radiology Department, School of Medicine, Johns Hopkins University, Baltimore, USA

Introduction

Nanomaterials are currently influencing a lot of our daily lives (Abbas et al. 2009; Adeleye et al. 2016). Of these, inorganic nanoparticles comprise of those which do not directly influence but indirectly improve our interaction with the world around us (Biyela et al. 2014; Chen et al. 2011; Huang et al. 2015; Johnston 2005). Inorganic nanocomposites are a mixture of individually prepared nanoparticles combined at different concentrations (Ivanov et al. 2003) as opposed doping (Rajendar et al. 2013) or substitution (Ahmadipour et al. 2012; Rajendar et al. 2014a, b, 2016a). These particles would gallop the properties of both the nanoparticles simultaneously while retaining their individual characteristics. There have been multiple reports of these composites which perform dually well when combined that in their individual states (Ivanov et al. 2003; Flahaut et al. 2000; Granqvist 1993). This property is of great use in the medical field where the use of nanocomposites could relatively increase the performance of two individual nanoparticles just by combining them. Synergistic application of multiple drugs are common among the medical field where two individual medications fail to produce a desired effect disjointedly, while inducing potent effects when combined together (Fried et al. 2002; Hurwitz et al. 2004).

The premise of using composite materials stems from the fact that zinc oxide (ZNPs) and titanium dioxide nanoparticles (TNPs) induce potent antibacterial and anticancer activities when applied in mill molar concentrations (Jones et al. 2008; Yamamoto 2001; Zhang et al. 2007; Brunet et al. 2009; Han et al. 2016; Montazer et al. 2011; Savvova and Bragina 2010). We have previously demonstrated potent antibacterial and anticancer activities of ZNPs and TNPs prepared by multiple synthesis routes

(Rajendar et al. 2014a, 2016a; Rajendar et al. 2016b, c; Li et al. 2012). Of these, we have shown potent activity in case of those prepared using Tween 80 as the surfactant (Rajendar et al. 2016b, c). Thus, produced nanoparticles seem to perform to a greater extent that those previously studied.

In this study, we have used a mixture of ZNPs and TNPs prepared by TWEEN 80 surfactant method and observed their antibacterial and anticancer properties via zone of inhibition and MTT assays. The particle mixtures were analyzed for their physiochemical properties before they were evaluated for the above mentioned assays.

Materials and methods

Synthesis of ZNP/TNP nanocomposites

The method of preparation of ZNPs and TNPs has previously been reported (Rajendar et al. 2016b, c). Thus, prepared nanoparticles were weighed and suspended in deionized (DI) water to initiate the mixing process. The particles were homogenized using Sonication for a period of 30 min at 20 kHz and Ultra Sound Power: 60–90 W. Mixing ratios of 1:1, 1:2, 1:3, 2:1, 2:3, 3:1, and 3:2 wt% ZNPs: TNPs were used in this study. Post homogenization, the samples were centrifuged at 2000 rpm for 30 min to pellet the nanocomposite mixture. These samples were then dried overnight at 100 °C in an oven to realize while crystalline nanocomposite powder.

Characterization techniques

Materials were characterized using field emission scanning electron microscopy and energy dispersive spectroscopy (FESEM&EDS) and images were taken at 1 μm magnification. JEOL JEM-2010 (HT) transmission electron microscopy (TEM) was used to analyze particle morphology and particle size analysis and the images were taken at 200 kV accelerating voltage. Dynamic light scattering (DLS) was performed on samples suspended in ethanol using a YD-laser (532 nm) and the mean value of the obtained histogram was considered the average particle size. Fourier transform infrared spectroscopy (FTIR) was performed for wavelengths 500–4000 cm^{-1}. X-ray diffraction studies were performed between 2θ values 20° and 80°. The samples were then analyzed for their average crystallite using the modified Debye Scherrer's formula.

Antimicrobial assay

The antimicrobial assays were performed using standard disc diffusion assay method, the process for which has been explained elsewhere (Rajendar et al. 2016b, c). *B. Subtilis*, *S. Aureus*, *E. Coli*, *and C. Albicans* were used as model Gram-negative and Gram-positive bacteria for this study. The nanocomposite concentrations used were 0.02, 0.04, 0.06, 0.08, 0.1, and 0.12 mg/μL. Only 1:1 ZNP/TNP samples were utilized in this study.

Anticancer activity

The anticancer activity was evaluated by performing MTT assay on four different non-additive cell lines, namely: human cervical cancer cell line (HeLa), Chinese hamster ovary cells (CHO), human breast adenocarcinoma cell line (MD-231), and Mus musculus skin melanoma cell line (B16-F10). Briefly, cells were plated in a 96-well plate at a seating density of 2×10^4 per well and left

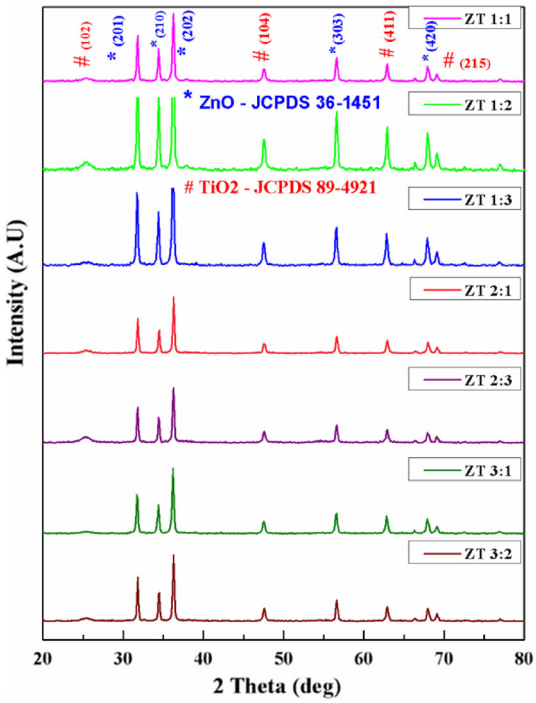

Fig. 1 2D XRD Plot of ZNP/TNP nanocomposite at different wt%

Table 1 Average crystallite size of ZNP/TNP nanocomposites at different wt%

Sample	Average crystallite size (nm)
ZT 1:1	15.3
ZT 1:2	18.5
ZT 1:3	19.8
ZT 2:1	18
ZT 2:3	22.2
ZT 3:1	20.3
ZT 3:2	25

overnight until they were 80% confluent (ELx-800 Absorbance Microplate reader). Various concentrations of the nanocomposite (1, 3, 10, 30 100 µg/mL) and control (PBS) were added to each well and were allowed to incubate for a period of 24 h at 37 °C and 5% CO_2. Post incubation, wells were washed with PBS twice before 100 µL of 0.5 mg/mL MTT (3-(4,5-dimethylthiazol-2-yl)-2,5-diphenyltetrazolium bromide) was added to each well and incubated for 4 h. Formazan crystals formed due to the mitochondrial activity were dissolved using acidified isopropanol (0.1% TrisHCl in isopropanol) and transferred to a new 96-well plate. The samples were analyzed by a Plate reader at 562 nm. Experiments were conducted in triplicates and individually repeated five times to compensate for pipetting errors. Only 1:1 ZNP/TNP samples were utilized in this study.

Results and discussions

Structural analysis of ZNP/TNP nanocomposite

The XRD pattern of ZNP/TNP nanocomposite is shown in Fig. 1. The XRD pattern shows Anatase TiO_2 peaks at 25°

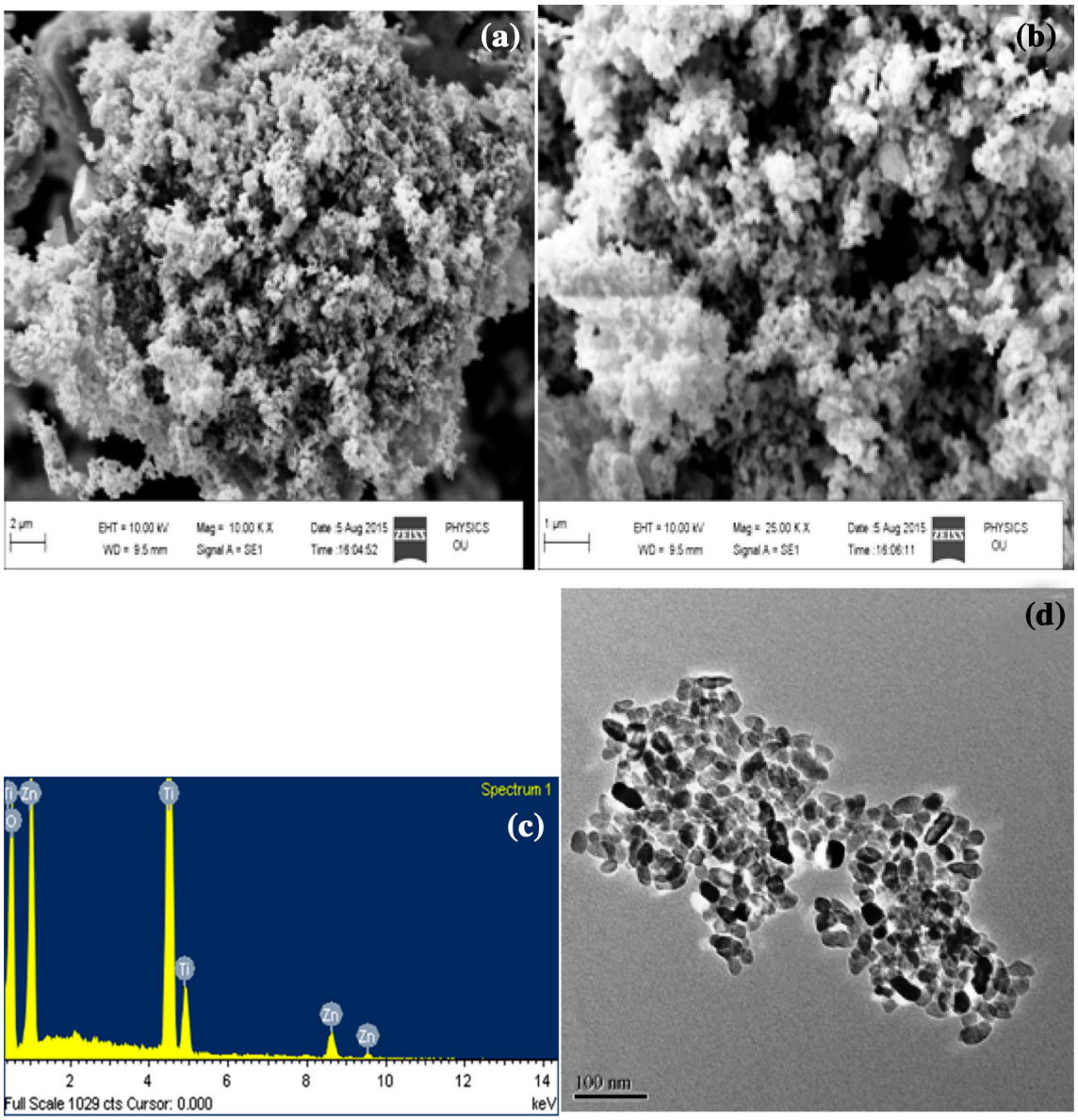

Fig. 2 **a–c** ZNP/TNP nanocomposite (1:1): FESEM images at 2 and 1 µm magnification (**a**, **b**) and its EDS spectrum (**c**). **d–g** ZNP/TNP nanocomposite (1:1): TEM images at 100, 20, and 10 nm magnification (**d–f**) and its SAED pattern. **h** Particle size distribution of ZNP/TNP nanocomposite (1:1)

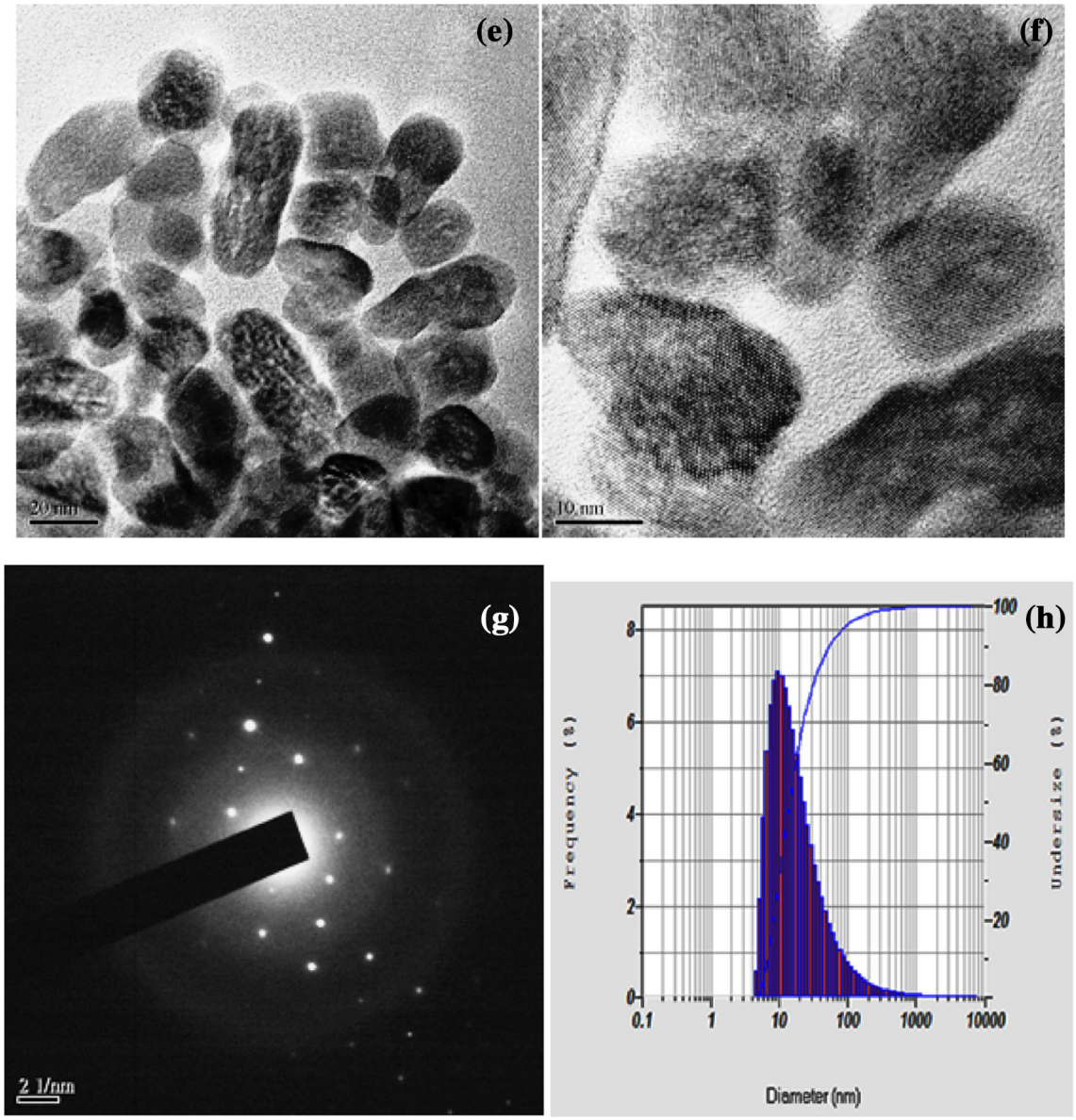

Fig. 2 continued

with increasing concentration of TiO_2 in the nanocomposite. In the figure, ZnO (Hexagonal) and TiO_2 (Tetragonal) phases were observed. These peaks were in good agreement with the standard diffraction card numbers (JCPDS) of ZnO and TiO_2 as 36–1451 and 89–4921, respectively. Each peak having different 2θ positions corresponding to crystalline planes (hkl).

The average crystallite sizes for these samples were analyzed by Debye–Scherrer's formula [$D = K \times \lambda/(\beta \cos \theta)$] and the results are indicated in Table 1. β is the full width half maximum (FWHM) of the XRD corresponding peaks, K is Debye–Scherer's constant, D is crystallite size, λ is wave length of the X-ray, and θ is Bragg angle.

Morphology and particle size analysis

The morphology of the nanocomposite at ZNP/TNP 1:1 ratio was evaluated by FESEM, TEM, and dynamic light scattering equipment. FESEM images (Fig. 2a, b) show globule-like particles along with unstructured particles present in the sample. The same is iterated in the TEM (Fig. 2d–g) showing an equal quantity of globule shaped particles with variable shaped particles. The globule shaped particles were confirmed to be ZNPs, while unstructured particles were shown to be TNPs by energy dispersive X-ray spectroscopy (Fig. 2c; Table 2) provided along with the FESEM. It is interesting to note that the dynamic light scattering analysis revealed the particle size to be in the

Table 2 EDS spectrum of ZNP/TNP nanocomposite (1:1)

Element	Weight	Atomic %
O K	37.2	66.35
Ti K	39.17	23.33
Zn K	23.63	10.31
Total	100	

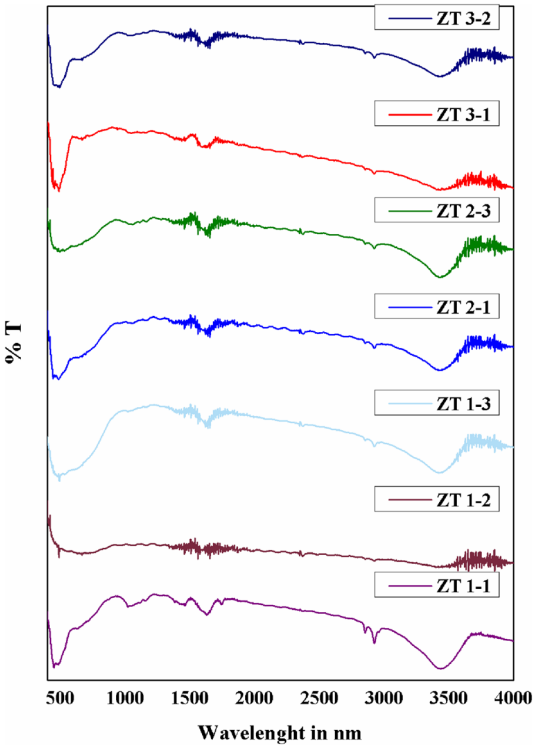

Fig. 3 FTIR of ZNP/TNP nanocomposite at different wt%

range of 26 nm (Fig. 2h) which is close to those measured by TEM.

Fourier transform infrared spectroscopy (FTIR) analysis

In Fig. 3, the FTIR spectra of ZNP/TNP nanocomposite can be observed. The wavelength range measured was from 500 to 4000 cm^{-1}. The broad absorption at low frequency at 500 cm^{-1} could be attributed to the Ti–O bonding. C–O stretching is observed at 1195 cm^{-1}, C–C stretching is observed at 1460 cm^{-1}, C=C stretch stretching is observed at 1690, 1730 cm^{-1}. Zn–O bonding is observed at 2850 and 2960 cm^{-1}, and O–H stretching at 3500 cm^{-1} (shown in Table 3). From this, we can confirm purity of the prepared samples without any unforeseen impurities. It can be hence stated that while varying wt% of ZNP/TNP nanocomposite, i.e., 1:1, 1:2, 1:3, 2:1, 2:3, 3:1, and 3:2 wt%, same functional groups were observed in all.

Table 3 FTIR spectrum of ZNP//TNP nanocomposite

Wavenumber (cm^{-1})	Bonding
500	M–O (M=Ti)
1195	C–O stretch
1460	C–C stretch
1690, 1730	C=C stretch
2850, 2960	N–O (N=Zn)
3500	O–H stretch

Antimicrobial assay

Zone of inhibition for ZNPs alone, TNPs alone, and ZNP/TNPs has been evaluated individually at different concentrations. The quantified values of the zone inhibition (ZI) are shown in Figs. 4, 5, and 6. It is clearly evident from the assays that ZNPs have a lower antibacterial action when compared to TNPs. This could be attributed to the spontaneous mutation caused by TNPs in bacterial samples as opposed to the reactive oxygen species-based mechanism explained for ZNPs (Li et al. 2012). However, it is interesting to note that the antibacterial activity of ZNP/TNP nanocomposite significantly increases when compared to ZNPs alone while decreases to a small extent when compared to TNPs. This result is important, because TNPs are known to cause genetic mutations in human beings when applied in higher quantities as opposes to the biocompatible and non-toxic property of ZNPs. Hence, we could say that the use of ZNP/TNP composite would significantly improve the antibacterial property of ZNPs while lowering the toxic range of TNPs.

Anticancer activity

The MTT assay for the ZNP/TNP nanocomposite can be seen in the Fig. 7a and b. Similar to the antibacterial assay, the anticancer properties of the nanocomposite seem to complement the ZNPs while having lower activity when compared to those of TNPs. This would mean that a composite material would significantly alter the methodology through which anticancer activities could be governed without compromising on the biocompatibility issues. Another important thing to note through these experiments is that except for CHO cell line, TNPs showed lower anticancer activity when compared to ZNPs at all concentrations. Furthermore, ZNPs had really low anticancer activity against the CHO cell line when compared to other cell lines. However, ZNP/TNP nanocomposite showed significantly high and equivalent anticancer activity against all the cell lines. And

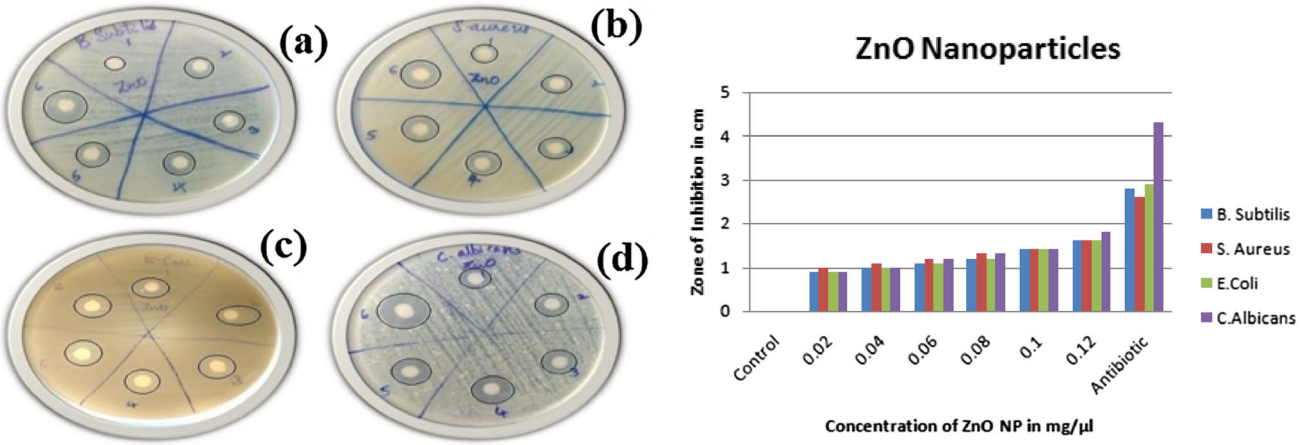

Fig. 4 Antibacterial tests: ZNPs ZI growths of (**a**) *B. subtilis,* (**b**) *S. aureus,* (**c**) *E. coli*, (**d**) *C. albicans* and respective bar diagram of ZI growths

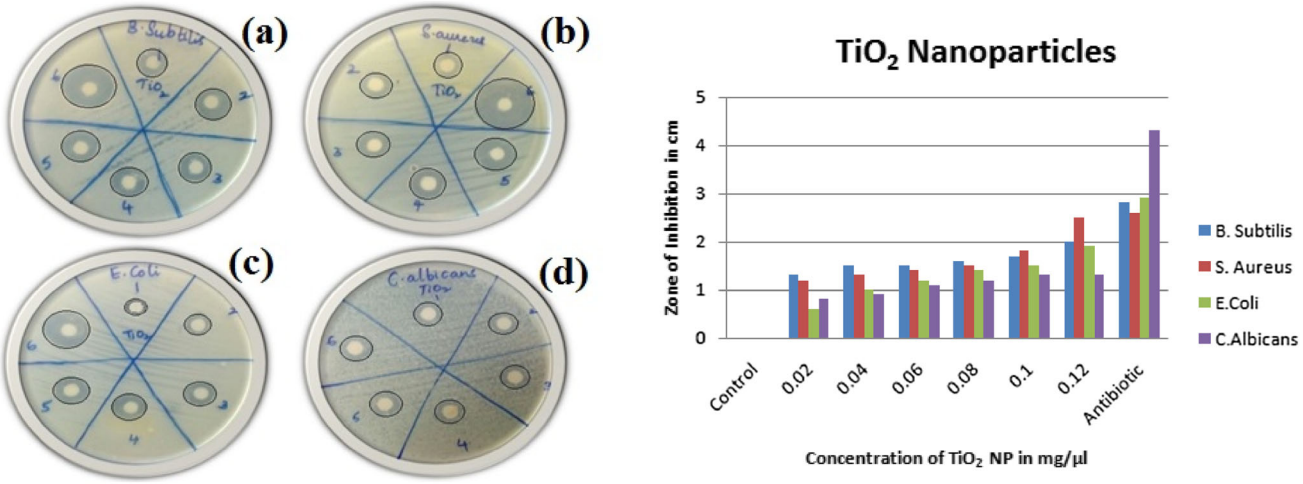

Fig. 5 Antibacterial tests: TNPs ZI growths of (**a**) *B. subtilis,* (**b**) *S. aureus,* (**c**) *E. coli*, (**d**) *C. albicans* and respective bar diagram of ZI growths

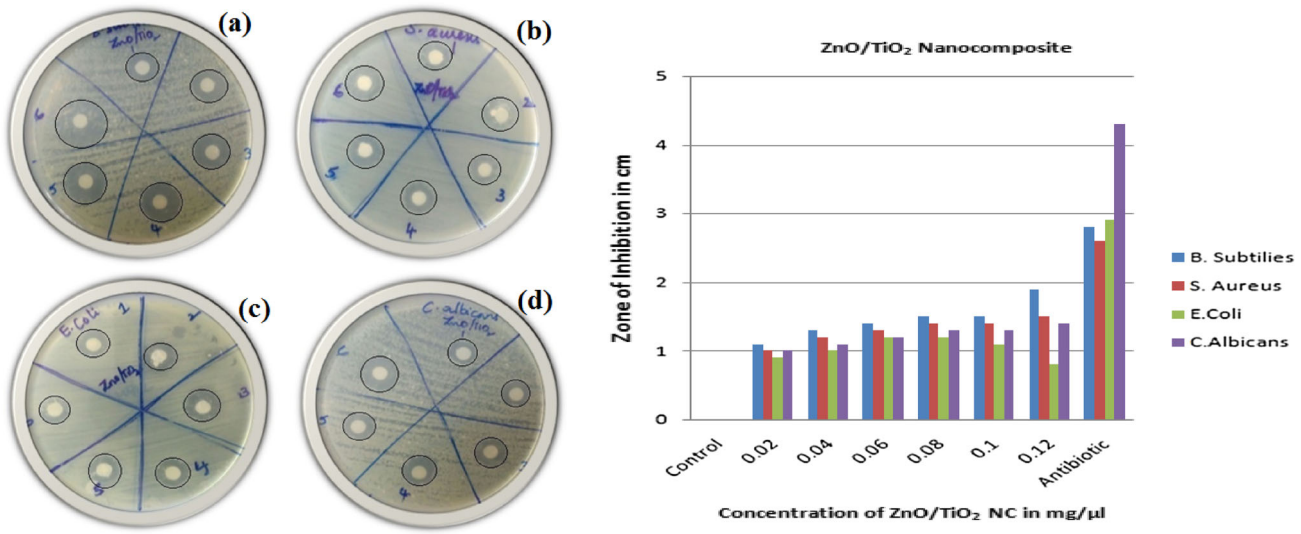

Fig. 6 Antibacterial tests: ZNP/TNP nanocomposite ZI growths of (**a**) *B. subtilis,* (**b**) *S. aureus,* (**c**) *E. coli*, (**d**) *C. albicans* and respective bar diagram of ZI growths

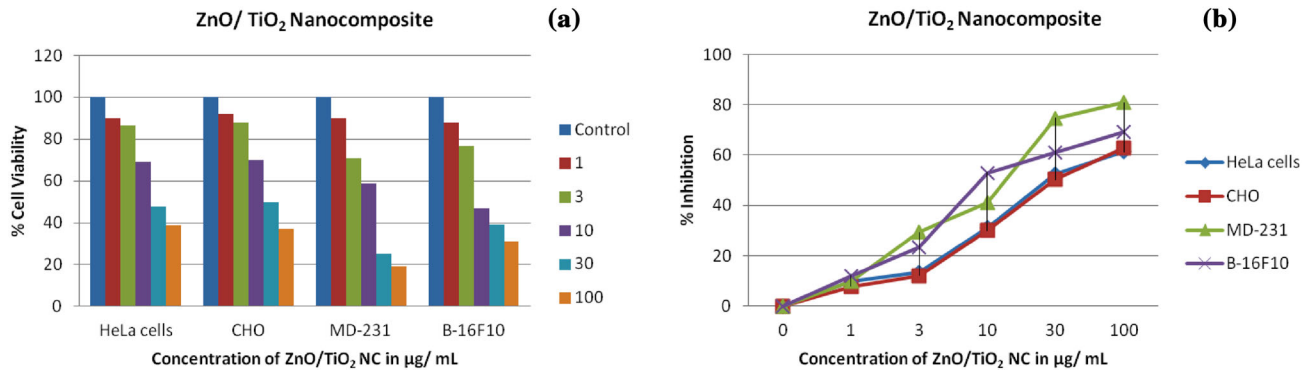

Fig. 7 **a** Percentage of cell viability with ZNP/TNP NC against HeLa, CHO, MD-231, and B-16F10 cancer cells (bar diagram). **b** Percentage of inhibition vs concentration of ZNP/TNP NC in µg/mL against MD-231 cancer cells

Table 4 Percentage of cell viability with ZNP/TNP NC against HeLa, CHO, MD-231, B-16F10 cancer cells

ZNP/TNP NC	% Cell viability			
Conc in µg/mL	HeLa cells	CHO cells	MD-231 cells	B-16F10 cells
Control	100	100	100	100
1	89.97	92.18	89.97	87.94
3	86.4	87.94	70.62	76.55
10	68.92	69.96	58.97	46.95
30	47.59	49.62	25.28	38.96
100	38.61	37.2	19.2	30.95

the percentage of inhibition versus concentration against cancer cells shown in Table 4. This implies that through the use of nanocomposites, the disadvantages offered by one particle can be compensated by the other particle used in the sample.

Conclusions

Nanocomposites of zinc oxide nanoparticles and titanium dioxide nanoparticles were made and tested for their antibacterial and anticancer properties. The results indicated an elevated antibacterial property for the nanocomposite when compared to zinc oxide but diminished property compared to titanium dioxide. In contrast, a diminished anticancer property was observed for the nanocomposite compared to zinc oxide, while an increased anticancer property when compared to titanium dioxide. However, bacterial types and cancer cell lines which were unaffected by either of the nanoparticles individually had an elevated antibacterial or anticancer property for the nanocomposite. This implicates those similar to medical drugs, which have synergistic properties when used against a certain disease, nanoparticles also show a synergistic effect when applied as composites. Our goal would be to further this research by testing various other combinations of composites and compare them to their individual nanoparticles.

Acknowledgements The authors are graceful to Prof. CH. Sasikala, Center for Environment, Institute of Science and Technology, JNT University Hyderabad, India, for providing the research facilities to undertake this work.

Compliance with ethical standards

Conflict of interest Dear Editor, I would like to inform you that we do not have any conflict of interest.

References

Abbas KA, Saleh AM, Mohamed A, Mohdazhan N (2009) The recent advances in the nanotechnology and its applications in food processing: A review. J Food Agric Environ 7(3–4):14–17

Adeleye AS, Conway JR, Garner K, Huang Y, Su Y, Keller AA (2016) Engineered nanomaterials for water treatment and remediation: costs, benefits, and applicability. Chem Eng J 286:640–662

Ahmadipour M, Rao KV, Rajendar V (2012) Formation of nanoscale $Mg_{(x)}Fe_{(1-X)}O$ (x = 0.1,0.2,0.4) structure by solution combustion: Effect of fuel to oxidizer ratio. J Nanomater 163909:1–8

Biyela PT, Lin J, Bezuidenhout CC (2014) The role of aquatic ecosystems as reservoirs of antibiotic resistant bacteria and antibiotic resistance genes. Water Sci Technol 50(1):45–50

Brunet L, Lyon DY, Hotze EM, Alvarez PJJ, Wiesner MR (2009) Comparative photoactivity and antibacterial properties of C60 fullerenes and titanium dioxide nanoparticles. Environ Sci Technol 43(12):4355–4360

Chen Y, Fan H, Shi B (2011) Nanotechnologies for leather manufacturing: A review. J Am Leather Chem Assoc 106(8):260–273

Flahaut E, Peigney A, Laurent C, Marlière C, Chastel F, Rousset A (2000) Carbon nanotube–metal–oxide nanocomposites: microstructure, electrical conductivity and mechanical properties. Acta Mater 48(14):3803–3812

Fried W, Shiffman ML, Reddy KR, Smith C, Marinos G et al (2002) Peginterferon alfa-2a plus ribavirin for chronic hepatitis C virus infection. New Engl J Med 347(13):975–982

Granqvist CG (1993) Electrochromic materials: metal oxide nanocomposites with variable optical properties. Mater Sci Eng A 168(2):209–215

Han C, Lalley J, Namboodiri D, Cromer K, Nadagouda MN (2016) Titanium dioxide-based antibacterial surfaces for water treatment. Curr Opin Chem Eng 11:46–51

Huang S, Wang L, Liu L, Hou Y, Li L (2015) Nanotechnology in agriculture, livestock, and aquaculture in China. A review. Agron Sustain Dev 35(2):369–400

Hurwitz H, Fehrenbacher L, Novotny W, Cartwright T, Hainsworth J, Heim W et al (2004) Bevacizumab plus irinotecan, fluorouracil, and leucovorin for metastatic colorectal cancer. New Engl J Med 350(23):2335–2342

Ivanov EY, Grigorieva TF, Barinova AP, Boldyrev V (2003) On the formation of metal-oxide nanocomposites by mechanochemical interaction. J Metastab Nanocryst Mater 15–16:569–572

Johnston N (2005) Novel approach to combating superbugs. Drug Discov Today 10(3):163–164

Jones N, Ray B, Ranjit KT, Manna AC (2008) Antibacterial activity of ZnO nanoparticle suspensions on a broad spectrum of microorganisms. FEMS Microbiol Lett 279(1):71–76

Li Yang, Zhang Wen, Niu Junfeng, Chen Yongsheng (2012) Mechanism of photogenerated reactive oxygen species and correlation with the antibacterial properties of engineered metal-oxide nanoparticles. ACS Nano 6(6):5164–5173

Montazer M, Pakdel E, Behzadnia A (2011) Novel feature of nano-titanium dioxide on textiles: Antifelting and antibacterial wool. J Appl Polym Sci 121(6):3407–3413

Rajendar V, Rao KV, Ahmadipour M, Shoban K (2013) Nanocrystalline $Zn_{1-x}Co_xO$ ($0.05 \leq x \leq 0.2$) Powders Produced by Novel Auto-Combustion Method and Their Characterization. Adv Sci Eng Med 05(11):1176–1180

Rajendar V, Dayakar T, Shobhan K, Srikanth I, Rao KV (2014a) Systematic approach on the fabrication of Co doped ZnO semiconducting nanoparticles by mixture of fuel approach for Antibacterial applications. Superlattices Microstruct 75:551–563

Rajendar V, Raju NP, Rao KV (2014b) Novel Ammonium Acetate Fuel Based Autocombustion Method for the Preparation of Nickel Doped Zinc Oxide Nanoparticles. Adv Sci Eng Med 5:683–687

Rajendar V, Rajitha B, Dayakar T, Chakra CHS, Rao KV (2016a) Systematic approach on the fabrication of Mn doped ZnO semiconducting nanoparticles by mixture of fuel approach for antibacterial applications. Rendiconti Lincei 27(3):521–531

Rajendar V, Chakra CHS, Rajitha B, Rao KV et al (2016b) Effect of TWEEN 80 on the morphology and antibacterial properties of ZnO nanoparticles. J Mater Sci Mater Electron 28(4):3272–3277

Rajendar V, Chakra CHS, Rajitha B, Rao KV, Park S (2016c) Role of Tween 80 as surfactant in the solution combustion synthesis of TiO_2 nanoparticles. J Mater Sci Mater Electron 28(4): 3394–3399

Savvova OV, Bragina LL (2010) Use of titanium dioxide for the development of antibacterial glass enamel coatings. Glass Ceram 67(5–6):184–186

Yamamoto O (2001) Influence of particle size on the antibacterial activity of zinc oxide. Int J Inorg Mater 3(7):643–646

Zhang L, Jiang Y, Ding Y, Povey M, York D (2007) Investigation into the antibacterial behaviour of suspensions of ZnO nanoparticles (ZnO nanofluids). J Nanopart Res 9(3):479–489